Pure Appl. Chem., Vol. 81, No. 3, pp. 495–511, 2009.
doi:10.1351/PAC-CON-08-08-15

Hydrophobicity recovery of corona-modified superhydrophobic surfaces produced by the electrospinning of poly(methyl methacrylate)-graft-poly(dimethylsiloxane) hybrid copolymers*

Morne Swart and Peter E. Mallon‡

Department of Chemistry and Polymer Sciences, University of Stellenbosch, Stellenbosch, Private Bag X1, Matieland, 7602, South Africa

Abstract: Superhydrophobicity is dependent on both the surface energy and the texture of the surface. These factors are discussed in terms of a series of electrospun poly(methyl methacrylate)-graft-poly(dimethylsiloxane) (PMMA-*g*-PDMS) copolymers with different poly(dimethylsiloxane) (PDMS) content. These copolymers are synthesized via conventional free radical copolymerization of methyl methacrylate (MMA) and monomethacryloxypropyl-terminated PDMS macromonomers. It is shown how these copolymers can be electrospun to produce copolymer fibers with diameters in the 100–1000 nm range. The effect of the copolymer composition (and hence the surface energy) and the electrospinning tip-to-collector distance (TCD) on the fiber morphology is discussed. The surfaces produced by the electrospinning process show superhydrophobic properties where the preferential surface segregation of the PDMS component is combined with the roughness of the fiber surface. The surface energy of the fibers is varied by variation of the PDMS content in the copolymers as well as by post-spinning modification with corona discharge. The hydrophobicity of the surfaces shows a greater dependence on the PDMS content than on the average fiber diameter. After exposure of these fiber surfaces to corona discharge, the initial superhydrophobic surfaces become easily wettable despite the fact that much of the surface roughness is maintained after exposure. The samples show the phenomena of hydrophobocity recovery after corona exposure. The rate and extent of this recovery depends on the PDMS content and the corona exposure time. Despite the recovery, scanning electron microscopy (SEM), swelling measurements, and confocal Raman spectroscopy show that permanent surface changes have taken place. The surfaces do not recover to their original superhydrophobic state.

Keywords: electrospinning; superhydrophobicity; hydrophobicity recovery; organic–inorganic hybrid polymers; surface properties.

INTRODUCTION

Superhydrophobic surfaces can be classified as those surfaces with a contact angle above 150° [1,2]. Materials with superhydrophobic surfaces are attracting much attention in the scientific community.

*Paper based on a presentation at POLYCHAR 16: World Forum on Advanced Materials, 17–21 February 2008, Lucknow, India. Other presentations are published in this issue, pp. 389–570.

‡Corresponding author: Tel.: +27 21 8082971; Fax: +27 21 8084967; E-mail: pemallon@sun.ac.za

These surfaces, also known as lotus effect surfaces (because superhydrophobicity was first observed in nature on the leaves of the lotus plant) are self-cleaning [1,2]. This leads to the fact that chemical reactions in water, such as oxidation, are reduced on superhydrophobic surfaces. The surface energy of the materials controls the hydrophobicity of a flat surface, and, as a general rule, hydrophobicity will increase when the surface energy is lowered and decrease when surface energy is increased. In the case of superhydrophobic surfaces, the physical causes of superhydrophobicity are not only due to the surface energy (chemical nature of the surface) but also as a result of microtexture of the surface. There are two possible physical effects that influence the hydrophobicity and hence the contact angle: either the liquid follows the solid surface, or it leaves air inside the texture (the Wenzel or Cassie state) [1]. An increase in the surface area (due to the presence of microtexture) amplifies the natural hydrophobicity of the material. Therefore, the rougher the material the higher the contact angle and thus the more hydrophobic the material will be.

Techniques to manufacture superhydrophobic surfaces can be divided into two main categories. The first is to make rough surfaces from low-surface-energy materials and the second is to chemically modify a rough surface of a material to produce a low surface energy.

One of the first artificial superhydrophobic surfaces produced by using rough surfaces was reported by Onda et al. [3] in the mid-1990s. Since then, a number of very innovative ways have been used to manufacture these surfaces. Besides water repellency, other properties like color, transparency, flexibility, etc. have also been incorporated into these systems.

Several ways of roughening a surface can be used to produce superhydrophobic surfaces. They include mechanical stretching [4], laser plasma/chemical etching [5,6], lithography [7], sol-gel processing and solution casting [8], layer-by-layer and colloidal assembling [9], electrical and chemical reaction [10], and, more recently, electrospinning [11].

One group of materials that is of great interest is fluorocarbons. The reason for this is its extremely low surface energy. An effective way of using this material to produce superhydrophobic surfaces was put forth by Zang et al. [4]. They used mechanical stretching of tetrafluoroethylene (Teflon®) film. By doing so, the film consists of fibrous crystals with a large fraction of void space in the surface. Shiu and Kuo [5], on the other hand, used oxygen plasma to treat Teflon and thereby obtained a rough surface structure. Yabu and Shimomura [12] prepared a porous membrane by casting a fluorinated block polymer solution under humid atmospheric conditions. Another material readily used for its low surface energy is poly(dimethylsiloxane) (PDMS). To roughen the surface, Khorasani et al. [13] used CO_2-pulsed lasers as an excitation source. The contact angles obtained were in excess of 175°, and it was concluded that the hydrophobicity was due to the high porosity and chain ordering on the PDMS surface. Another popular method is to make a negative template out of an existing superhydrophobic material, like that of the lotus leaf. This is then used together with a nanocasting procedure to produce superhydrophobic PDMS materials.

Several methods exist to modify the surface energy of materials by modification of the surface chemistry to produce superhydrophobic surfaces [15]. The techniques that have been used include covalent bond formation between gold and alkyl thiols, the use of silanes, physical binding, adsorption, and coating. Teshima et al. [7] produced transparent superhydrophobic surfaces from a PET substrate by firstly etching it with oxygen plasma and then treating it with plasma-enhanced chemical vapor deposition using tetramethylsilane. Numerous other examples exist in literature. Techniques used in these instances include sol-gel processing [14], layer-by-layer and colloidal assembly [3], and electrical reaction and deposition [4].

As mentioned above, one method for producing polymer surfaces with very rough microtextual features is the electrospinning process. This technique can be used to make polymer nanofibers [16–20]. During the electrospinning process, a high voltage causes charges to be induced within the polymer solution. Above a certain critical point these charges cause a fluid jet to erupt from the tip of a pipette or needle. This results in the formation of a fluid cone. The jet thus formed will travel toward the grounded collector plate (which is the lower potential). There are a number of parameters that affect electro-

spinning and the resulting morphology of the polymer nanofibers. These parameters may be broadly classified into the effects of the polymer solution, processing conditions, and the ambient conditions used during the spinning process [21–23].

In this paper, we report on the ability of poly(methyl methacrylate)-graft-poly(dimethylsiloxane) (PMMA-*g*-PDMS) hybrid polymers to undergo electrospinning to form fibers with diameters in the range of 100–1000 nm. The graft copolymers described in this paper were prepared by free radical copolymerization and the "grafting through" macromonomer technique, using a monomethacryloxypropyl-terminated PDMS macromonomer. The PDMS content of the copolymers was varied by changing the macromonomer-methyl methacrylate (MMA) feed ratios in the copolymerization reaction [24].

These types of hybrid copolymers are very interesting due to the incompatibility of the PDMS and PMMA segments that leads to phase-segregated morphologies. Y. Lee et al. [25] have shown that a key property of PDMS is its low surface energy, which results in most polymer blends with PDMS having phase-segregated morphologies. They investigated the effect of polymer chain length on surface segregation of PMMA-*g*-PDMS/P(2EHA-AA-VAc) blends. The blends of PMMA-*g*-PDMS with P(2EHA-AA-VAc) showed surface segregation of the PDMS component. They concluded that the surface enrichment of PDMS in the blends depended on the PDMS chain length. More specifically, as the PDMS chain length in PMMA-*g*-PDMS increased the concentration of PDMS at the surface increased.

It is well known that PMMA homopolymer can readily be electrospun to form polymer nanofibers [26,27]. PDMS homopolymer cannot be electrospun due to its very low glass transition temperature. By producing a hybrid graft copolymer of PMMA and PDMS in this study, we found that the hard PMMA segments allowed the copolymers to be electrospun to produce nanofiber surfaces that contain a high percentage of PDMS. The surfaces produced in this way have the potential to show the phenomenon of "superhydrophobicity", where the static water contact angles exceed 150° due to the very rough surface and the hydrophobic nature of the PDMS component. Ma et al. [11] have shown that poly(stryrene-*b*-dimethylsiloxane) diblock copolymer synthesized via sequential controlled anionic polymerization of styrene followed by a ring-opening polymerization of hexamethylcyclotrisiloxane (D_3) could be electrospun after blending with polystyrene. This process produces superhydrophobic surfaces.

It is well known that exposure to corona discharge or other forms of plasma treatment can have significant effects on the surface energy of polymer samples [28–30]. Exposure of pure cross-linked PDMS compounds to corona discharge is known to lead to the phenomenon of hydrophobicity loss and recovery. Several researchers have studied the underlying molecular mechanisms of hydrophobic recovery in pure PDMS-based compounds. Using angle-resolved X-ray photoelectron spectroscopy (XPS), Owen and coworkers [31,32] found that a thin wettable, brittle silica-like layer was formed after corona treatment of PDMS in air. According to Hillborg et al. [33], hydrophobic recovery is usually explained as being due to a diffusion of unoxidized low-molar-mass PDMS through cracks in the silica-like surface layer. Toth et al. [34] studied silicone rubber surfaces exposed to plasma or corona discharges in air. They found that the diffusion of low-molecular-weight PDMS played a larger role toward hydrophobicity recovery than reorientation of polar groups in the bulk of the rubber. Morra et al. [35] used a combination of static secondary ion mass spectroscopy, XPS, and Fourier transform infrared (FTIR) spectroscopy on 0^{18} plasma-modified PDMS and proposed that the hydrophobicity recovery was due to the burial of polar groups into the bulk of the polymer and to surface condensation of silanols and consequent cross-linking in the contact angle probed layer. Hollahan [36] and Scott et al. [37] have also discussed certain chemical reactions that occur during corona discharge. Mallon et al. [38] used positron annihilation spectroscopy (PAS) to study the effects of high-voltage discharge on PDMS insulators. They concluded that high-voltage corona discharge leads to the formation of a brittle silica-like layer. Meincken et al. [39] used atomic force microscopy (AFM) force-distance curves to track the hydrophobicity recovery of PDMS polymers after exposure to corona discharge. They concluded that the adhesive force derived from the AFM curve can be used to track the recovery of the hydrophobicity

of these materials without the need for a water droplet to be in contact with the surface, as is the case with the static contact angle (SCA) measurements.

In this paper, we examine the effects of the surface morphology (or more specifically the electrospun fiber morphology) and the surface energy of the fibers. The surface energy of the fibers is changed in two ways.

EXPERIMENTAL

Copolymer synthesis

The free radical copolymerizations of different amounts of monomethacryloxypropyl-terminated PDMS macromonomer with MMA were performed in degassed toluene at 70 °C for 42 h using 0.1 wt % (based on MMA) azobis(isobutyronitrile) (AIBN) as initiator. The macromonomer had a molar mass of 800–1200 g/mol. The copolymer composition was varied by varying the MMA macromonomer feed ratio in the copolymerization reaction. The copolymerizations were carried out using 20 wt % solids (based on MMA). The PMMA-*g*-PDMS polymer was precipitated in methanol and the isolated copolymer extracted with *n*-hexane to remove excess PDMS macromonomer. The formation of the graft copolymers and the effective removal of the unreacted PDMS macromonomer were confirmed using gradient elution high-performance liquid chromatography (HPLC). A Nucleosil 100 Si 5-μm column was used, and the solvent gradient profile was varied from a 40 % [toluene/ethanol solution (90:10)] and 60 % cyclohexane starting solution to a 100 % toluene/ethanol solution. The PDMS content of the purified copolymers was determined using ^{1}H NMR spectroscopy. The spectra were recorded using a Varian Inova 600 MHz NMR spectrometer. The PDMS content was determined by integration of the δ 4.07 ppm peak of the O–CH_3 from the PMMA and the δ 0.5 ppm Si–CH_3 peak. The molar mass of the copolymers was determined by size exclusion chromatography (SEC) using a Waters HPLC system using two PL gel 5-mm mixed C (200 × 7.5 mm) columns and tetrahydrofuran (THF) as the mobile phase. The M_n, M_w, and PDI values are reported as relative to the linear polystyrene standards used to calibrate the system. A summary of the synthesized copolymers is given in Table 1.

Table 1 Summary of synthesized copolymer used in the study.

Sample	M_n (g/mol)	M_w (g/mol)	M_n/M_w	Wt % PDMS charged	Mol % PDMS charged	Mol % PDMS incorp via ^{1}H NMR
PMMA	89 689	174 616	1.95	~	~	~
5 wt % PDMS	78 172	130 190	1.67	5	0.66	0.29
10 wt % PDMS	146 255	268 360	2.08	10	1.46	0.57
15 wt % PDMS	69 983	154 331	2.20	15	2.18	1.14
23 wt % PDMS	95 654	284 623	2.98	23	3.62	1.91
34 wt % PDMS	101 405	354 527	3.50	34	6.08	3.88

Electrospinning procedure

A 10 wt % solution of the copolymer was prepared in a 60 % dimethylformamide (DMF) and 40 % chloroform mixture (V/V). The solution was placed in a glass pipette and gravity-fed through the tip. All samples were spun using a 0.5-mm tip opening. A copper wire electrode was inserted into the solution, and a grounded electrode was attached to an aluminum foil pan filled with water. The spun fibers were therefore collected on the surface of the water. A 25 kV, 400 micro amps (10 W) output high-voltage supply was used for the electrospinning process, and a voltage of 10 kV was applied and kept con-

stant for all samples. Two tip-to-collector distances (TCDs) were used in this study, namely, a 15- and 20-cm spinning distance.

Static contact angle measurements

SCAs were measured at room temperature and atmospheric pressure using distilled deionized water. All measurements are reported as the mean of at least 10 1-μL drops. The contact angles were determined from analysis of the digital images of the drops on the surface captured using a Nikon SMZ-2T light microscope fitted with digital image-capturing software. All images were captured immediately after placement of the drop on the surface.

Corona surface treatment

The samples were exposed to corona discharge for various times using a model BD-20C laboratory corona dischargers supplied by Electro-Technic products. The samples were placed at the bottom of a 1-L beaker, and the discharge needle was placed 10 mm from the sample surface.

Cross-link density determinations after exposure to corona

Electrospun fibers treated with high-voltage corona discharge were placed in THF at a concentration of 5 mg ml^{-1}. They were allowed to swell and reach equilibrium at room temperature for approximately 24 h. Thereafter, the samples were removed from the THF and weighed to determine the mass in the swollen state. The samples were then left to dry in a fume hood for 24 h and placed in a vacuum oven for an additional 2 h to remove any residual solvent. The mass of the dry sample was determined. The following equation was used to determine the volume fraction polymer in the swollen state at equilibrium, V_r:

$$V_r = \frac{m_r\, p_r^{-1}}{m_r\, p_r^{-1} + m_s\, p_s^{-1}}$$

where m_r is the residual mass (in grams) of the polymer after deswelling, m_s is the solvent mass (in grams) at equilibrium swelling, p_r is the density of PMMA-*g*-PDMS, and p_s is the density of THF.

Scanning electron microscopy (SEM)

SEM was used to establish the exact nature of the surface morphology as well as chemical composition using an energy-dispersive system (EDS). SEM analysis was performed on a Leo 1430VP SEM fitted with a backscatter, cathodoluminescence, variable-pressure and energy-dispersive detectors, as well as a link EDS system and software for microanalysis and qualitative work. The SEM system was designed to perform high-resolution imaging and quantitative analysis. The system had an error range of 0.5–0.2 wt % on the major elements.

RESULTS AND DISCUSSION

Table 1 shows a summary of the various copolymers synthesized and used in this study. The composition of the copolymers was determined using ^{1}H NMR spectroscopy after extraction of any PMMA homopolymer and unreacted PDMS macromonomer and is shown in Table 1. As expected, there is an increase in the PDMS copolymer content with an increase in the PDMS macromonomer feed ratio. All

the synthesized copolymers had M_n values in excess of 70 000 g/mol and M_w/M_n values of between 1.67 and 3.50.

The synthesized copolymers shown in Table 1 were electrospun to produce polymer fibers. Two different tip-to-collector spinning distances were used during the electrospinning. Varying the TCD will have a direct influence on the flight time and the electric field strength as well as the solvent evaporation rate and therefore influence the nature of the fibers [40]. The fiber diameter may also be influenced by the polymer solution concentration with more concentrated solution leading to larger fiber diameters [41,42]. In this study, the solution concentration and applied voltage were kept constant and only the copolymer composition and TCD were varied. Figures 1a–e show the SEM images as well as the distribution in the fiber diameters for the electrospun copolymer series with different PDMS content. The distribution in fiber diameter was determined by the analysis of at least 60 different fibers from the SEM images. Table 2 shows a summary of the fiber morphology for each of the electrospun copolymers and includes the average fiber diameter as well as the average bead size for the beaded samples. The Si/C ratio of the electrospun fibers determined using EDS for the 15-cm TCD is also shown in Table 2. In general, the closer spinning distance leads to fibers with larger diameters as well as a greater distribution in diameters than the 20-cm spinning distance. The 5 wt % PDMS content electrospun copolymers show the smallest fiber diameters, but in both the 15- and 20-cm spinning distances they produce a highly beaded fiber morphology. The average bead size in these samples is given in Table. 2. Lesser amounts of beading are observed in some of the other samples. There is an increase in the average fiber diameter with an increase in the PDMS content of the copolymers for each of the TCD series.

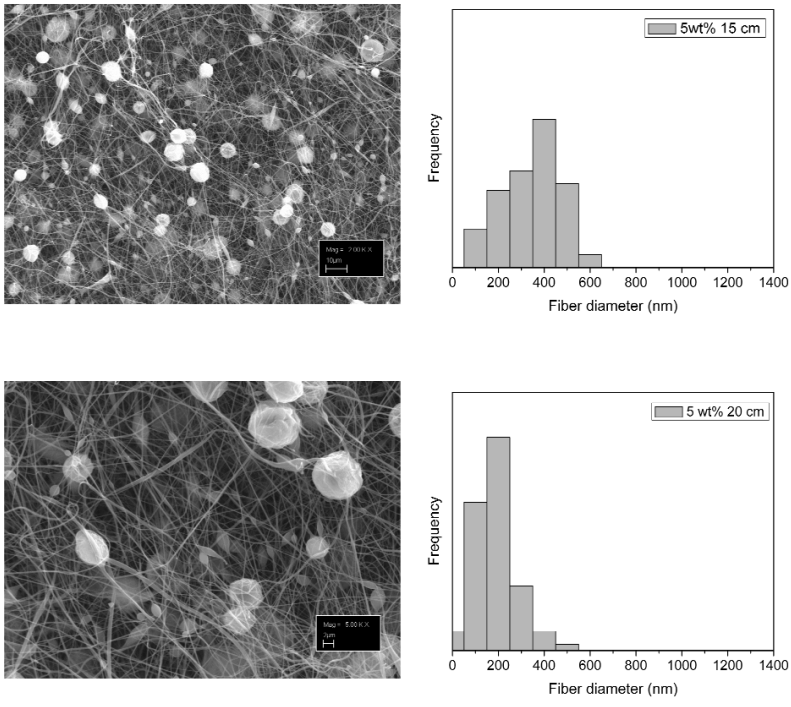

Fig. 1a SEM images and fiber diameter distribution for electrospun copolymers of different PDMS content and TCDs. 5 wt % PDMS copolymer.

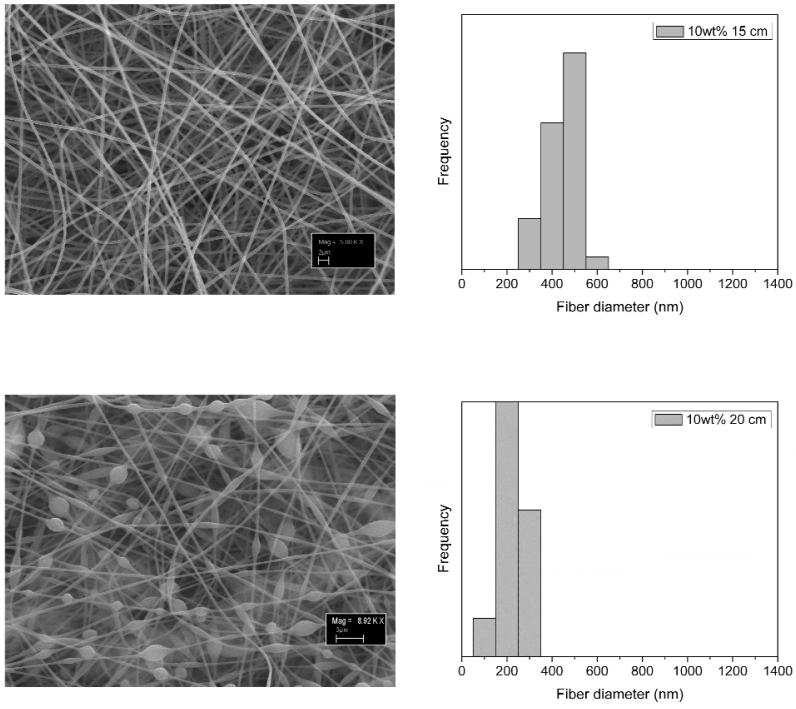

Fig. 1b SEM images and fiber diameter distribution for electrospun copolymers of different PDMS content and TCDs. 10 wt % PDMS copolymer.

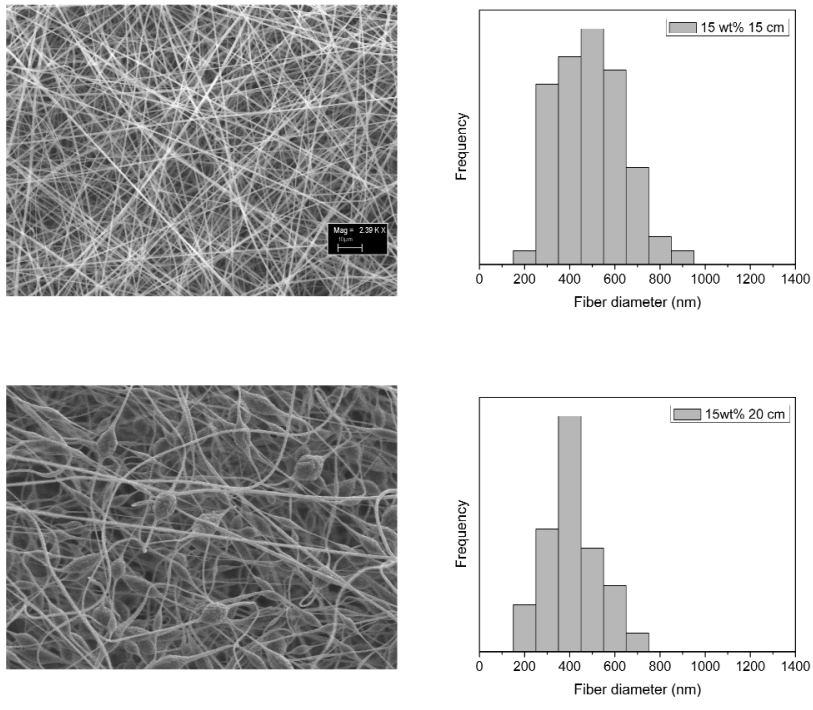

Fig. 1c SEM images and fiber diameter distribution for electrospun copolymers of different PDMS content and TCDs. 15 wt % PDMS copolymer.

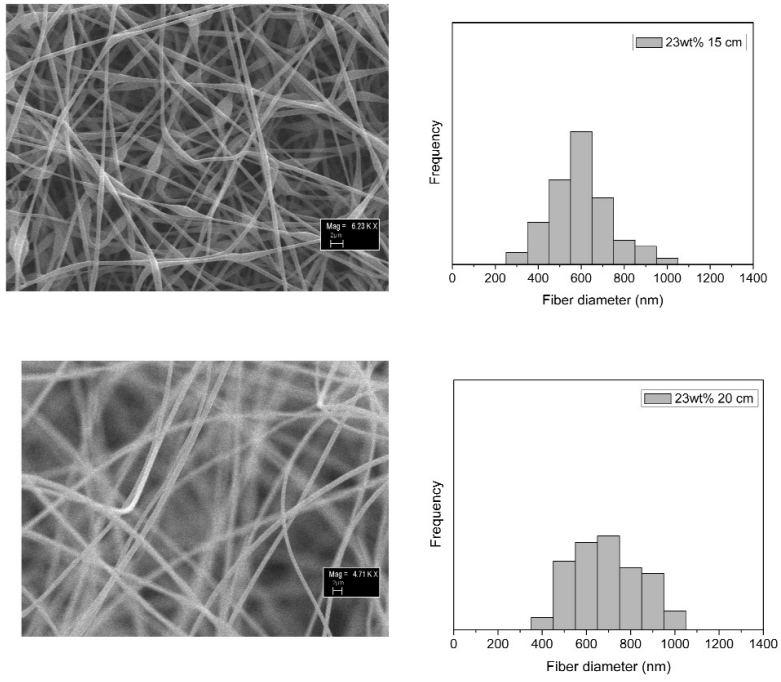

Fig. 1d SEM images and fiber diameter distribution for electrospun copolymers of different PDMS content and TCDs. 23 wt % PDMS copolymer.

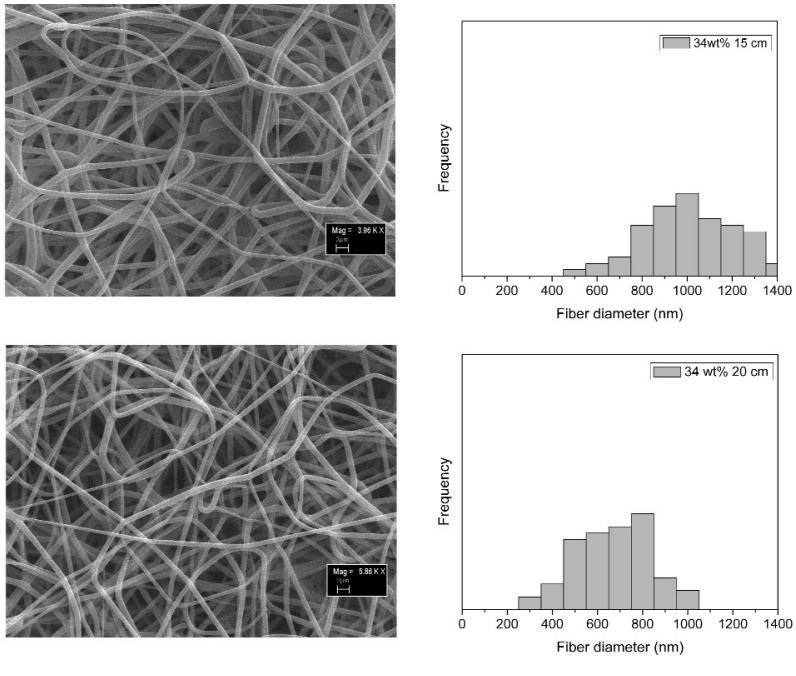

Fig. 1e SEM images and fiber diameter distribution for electrospun copolymers of different PDMS content and TCDs. 34 wt % copolymer.

Table 2 Fiber morphology.

	15-cm TCD		20-cm TCD		
Sample	Avg. fiber diameter (nm)	Average bead diameter (μm)	Avg. fiber diameter (nm)	Avg. bead diameter (μm)	Si/C ratio (15-cm TCD)
PMMA	546	–	389	–	–
5 wt % PDMS	395	3.2	231	2.3	0.0108
10 wt % PDMS	480	–	268	–	0.0201
15 wt % PDMS	537	–	459	2.6	–
23 wt % PDMS	807	1.7	751	–	0.0793
34 wt % PDMS	1092	–	725	–	0.1

Figure 2a shows the water SCA for the electrospun copolymers for both the TCD series as well as for the bulk copolymer films. Figure 2b shows selected images of the water drops for the 20-cm TCD series with increasing PDMS content. The increase in the contact angle for PDMS-based copolymer films is a well-known phenomena and the surface contact angle generally increases with the amount of PDMS since the PDMS component preferentially surface-segregates. The preferential surface segregation of PMDS in various copolymers and blends is well documented in the literature [25,43,44]. There is, however, a remarkable increase in the SCA measurement of the fiber surfaces relative to the copolymer films. Both the fiber series show the property of superhydrophobicity with SCAs greater than 150° especially for the higher-content PDMS copolymers. This increase in the SCA is indicative of the dramatic increase in the surface roughness of the electrospun surfaces relative to the copolymer films.

(a)

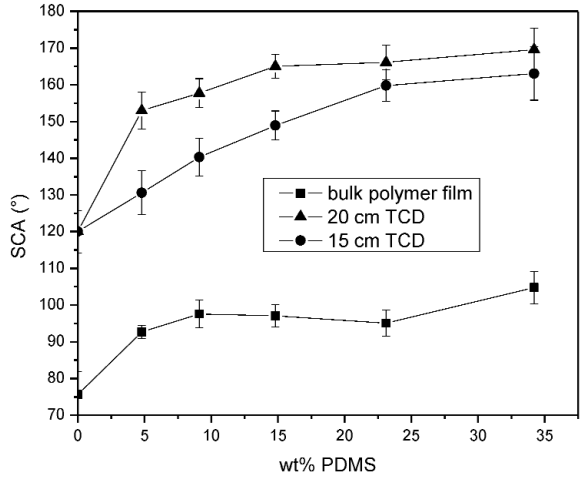

(b)

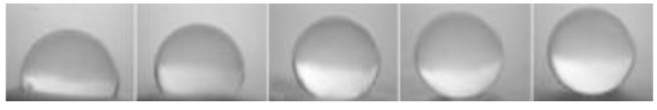

Fig. 2 (a) SCA for electrospun copolymer fiber surfaces and bulk copolymer films as a function of PDMS content. (b) SCA images of water drops on the surface of the 20-cm (TCD) copolymer fiber series.

Figure 3 shows the 3D plots of the relationship between the measured SCA, the PDMS content, and the average fiber diameters for both the TCD series. Generally, the SCA values are larger for the 20-cm TCD series than the 15-cm series. This is indicative of the fact that the 20-cm series produces surfaces with a smaller average fiber and, therefore, a "rougher" surface. There is also a greater dependence of the SCA on the PDMS content for the 15-cm series relative to the 20-cm series, with the 20-cm series showing superhydrophobicity for all copolymers, while the 15-cm series only show superhydrophobicity for PDMS content above 15 wt %. This can again be attributed to the difference in the average fiber diameter for the two series. The smaller fiber diameter in the 20-cm series effectively produces a larger surface area for these fibers. Since the PDMS component will preferentially surface-segregate, the larger surface area effectively means an increased PDMS content leading to higher SCA values.

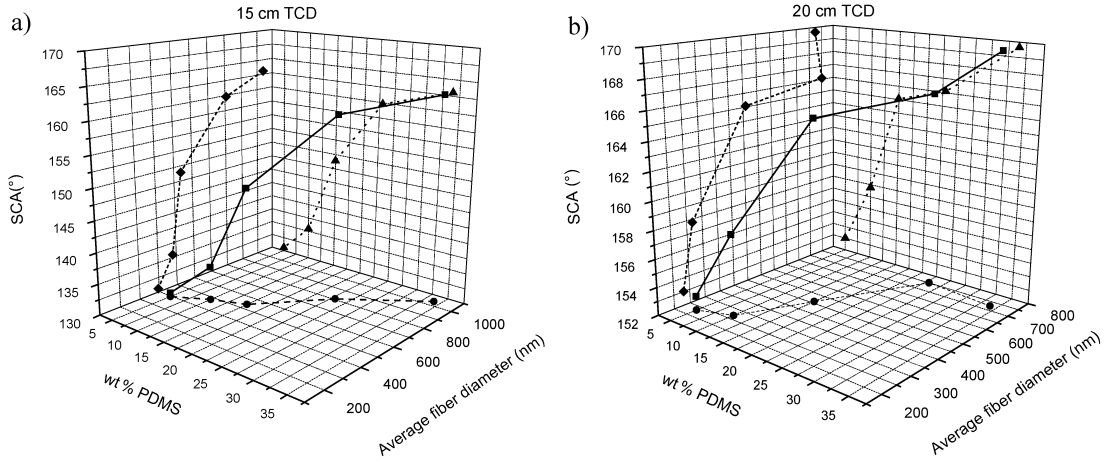

Fig. 3 3D plots of the relationship between the SCA, the PDMS content and the average fiber diameter for both the (a) 15-cm and (b) 20-cm TCD series.

From Fig. 3 it is clear that the PDMS content dominates the SCA rather than the average fiber diameter. As mentioned previously, the higher-content PDMS copolymers produce fibers of larger diameter (this is clearly seen in the wt % PDMS vs. average fiber diameter projections in Fig. 3). Despite the larger fiber diameters, the higher-content PDMS copolymers show greater SCAs. This means that the observed increase in the SCA is not entirely due to the fiber morphologies. When the copolymers are electrospun to form the nanofibers, the effective increase in the surface area magnifies the contribution of the PDMS components (which preferentially surface-segregate) beyond that of the copolymer films. This indicates that the electrospinning process is an effective means of producing "surfaces" of a progressively lower surface energy by variation of the PDMS wt %, whereas in the bulk films, the SCA reached a maximum more or less constant value at relatively lower PDMS content.

It is well known that exposure to corona discharge or other forms of plasma treatment can have a dramatic effect on the surface energy of polymer samples [37–39]. The effect of corona exposure on the nanofiber surfaces was investigated. Samples were subjected to varying times of corona discharge. Thereafter, contact angle measurements were performed on these treated samples. Directly after corona treatment, the superhydrophobic character of all the surfaces is completely lost and a contact angle of zero was obtained for all the samples directly after treatment. This change from superhydrophobicity to superhydrophilicity directly after corona treatment is illustrated in Fig. 4 for the 34 wt % electrospun surface where a series of images shows the effect of the corona treatment on a water droplet brought into contact with the surface directly after corona treatment. These images were captured over a 3.5 s

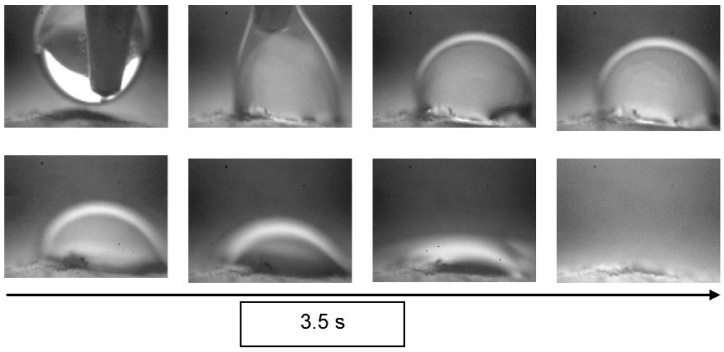

Fig. 4 Image capture of water drop in contact with 30-min corona-treated 34 wt % PDMS copolymer nanofiber surface immediately after exposure. The series of images were taken over a 3.5 s period.

period after the drop is brought into contact with the surface. The sample was corona-treated for 30 min. It can be seen that the water droplet is completely absorbed by the polymer fibers as soon as it is brought into contact with the surface. This is in stark contrast to the images of the water droplets on the untreated surface (shown in Fig. 2b) where the contact angle was 169°.

Figure 5 shows the SCA measurement of the surface as a function of the recovery time after corona exposure for different treatment times for the 34 wt % electrospun surface. It can be seen that the samples show the phenomena of "hydrophobicity recovery". This is typically observed in pure cross-linked PDMS compounds after corona treatment. The data shows that the exposure time has a dramatic effect on the recovery rate. In the case of the 34 wt % PDMS sample exposed to 2–10 min of corona, there is a rapid recovery in the first minutes after treatment. Recovery continues for approximately 2.5 h until the maximum SCA values are reached. This maximum value does not, however, return to 100 % of the initial SCA value before treatment, and these surfaces cannot be considered to be superhydrophobic after corona treatment and recovery. With longer corona treatment times, the rate of recovery is considerably slower. The 30-min corona-treated samples show no hydrophobicity recovery and remain completely wettable. The sample exposed to corona discharge for 20 min takes approxi-

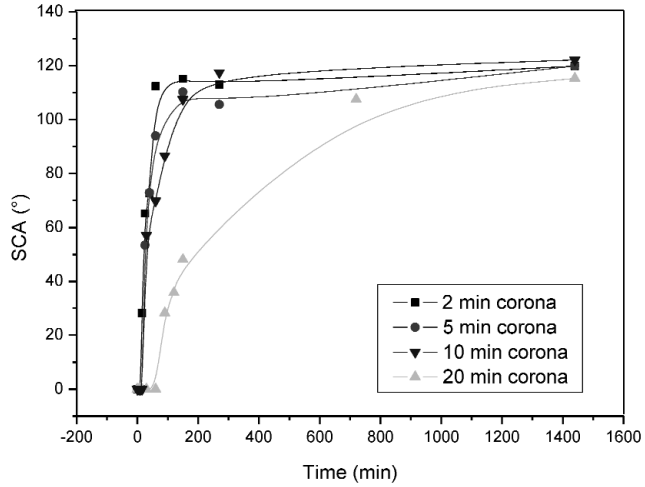

Fig. 5 SCA as a function of recovery time (time after corona exposure) for the 34 wt % electrospun surface, for different corona treatment times.

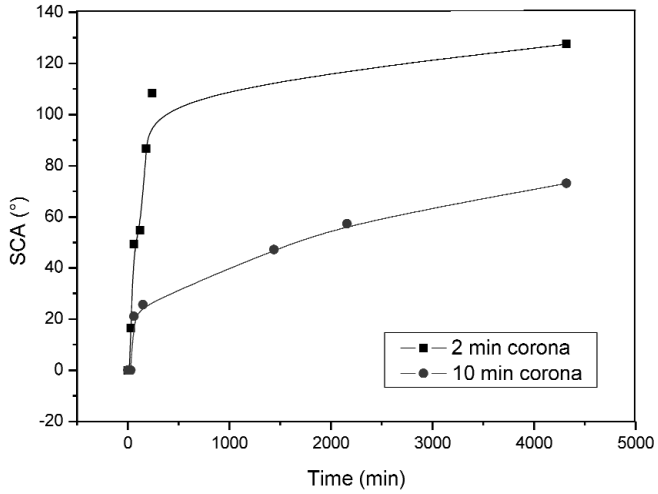

Fig. 6 SCA recovery of 10 wt % PDMS electrospun surface sample subjected to varying times of corona discharge.

mately 12 h to recover to its maximum value vs. the 2.5 h for the other samples. Figure 6 show a similar plot for the lower 10 wt % PDMS electropsun copolymer surface for two corona treatment times. These samples show the same general recovery trend, but over a much longer time period.

Several researchers have suggested that the diffusion of low-molecular-weight species (mostly cyclics) tends to be the dominant factor in hydrophobic recovery [33,34] observed in pure PDMS compounds. These low-molecular-weight species are formed in situ by degradation of the PDMS polymer during the corona exposure. The lower recovery rate for the 10 wt % sample in this study is most probably due to the lower PDMS content of these fibers which would result in the generation of fewer low-molecular-weight PDMS species which are most likely responsible for the hydrophobicity recovery observed.

In order to study the effects of corona treatment on the degradation of the copolymers, the corona-treated fibers were dissolved in THF. It was noted that after corona treatment the samples were insoluble, indicating that a cross-linking had taken place during corona exposure, making analysis of the change in molar mass by liquid chromatography impossible. Figure 7 shows the relationship between the cross-linking density (or V_r) and the corona treatment time. There is an initial increase in the cross-linking density at shorter treatment times and then a progressive decrease at longer treatment times. This suggested that in the initial stages of the corona treatment, polymer degradation leads to cross-linking in the fibers. Longer treatment times cause further breakdown in the polymer chains. During this process, low-molecular-weight PDMS compounds are formed and these are responsible for the SCA recovery observed.

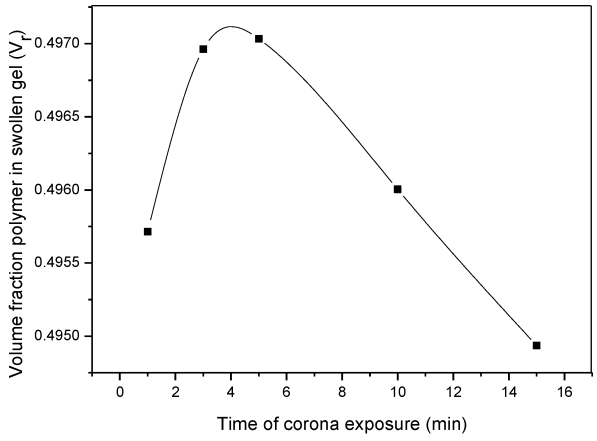

Fig. 7 Volume fraction polymer in the swollen state (V_r) for the 34 wt % electrospun copolymer for various corona treatment times.

Figure 8 shows the SEM images for the deswelled samples after the cross-link density determinations. It can be seen that after the swelling experiment, the fiber morphology is somewhat maintained in the treated samples. The results of the cross-link density experiments and the SCA recovery data indicate that after prolonged exposure to corona (>30 min) degradation of the polymer has occurred to such an extent that no low-molecular-weight components exist to aid in the recovery.

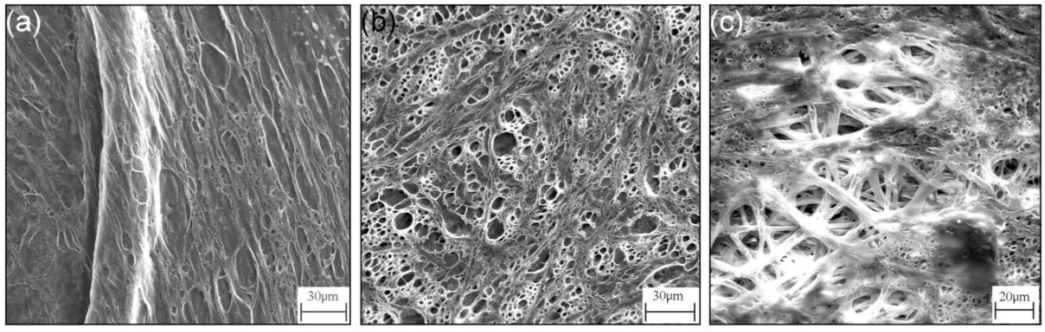

Fig. 8 SEM images of deswelled cross-linked samples after exposure to corona discharge. Figures show sample subjected to (a) 5 min, (b) 10 min, and (c) 15 min of corona exposure. All samples are 34 wt % PDMS sample.

Figure 9 shows the SEM images of the surface of the fibers change dramatically when exposed to the degradation effect of the ozone and electrical bombardment due to the corona discharge. Before exposure, all fibers show a smooth surface texture, but after exposure the surface of the fibers is extremely rough and irregular. Evidence is seen for the embrittlement of the fibers. A similar type of embrittlement in pure PDMS surface is observed after corona treatment and in these cases is often ascribed to the formation of a brittle SiOx-type layer after corona exposure [31–34,38]. Some areas show a region where the fibers have merged to form a smoother area.

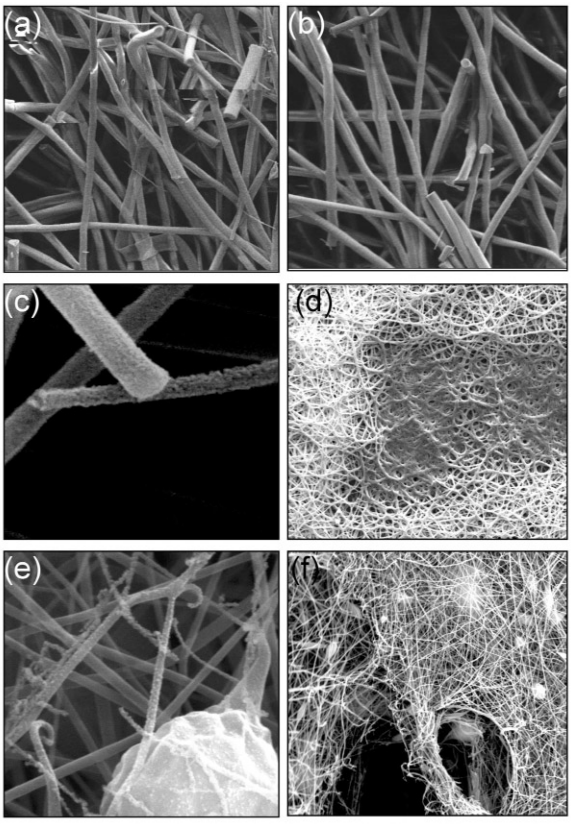

Fig. 9 SEM images illustrating the effects on fiber morphology after 30-min corona treatment. Images (a), (b), (c), and (f) show permanent fiber breakage and the formation of holes in the fiber mesh. Image (d) shows the fusion of fibers leading to an overall decrease in surface roughness, and images (c) and (e) show the rough nature of individual fibers not seen prior to corona treatment.

Confocal Raman spectroscopy was used to determine if any evidence of SiOx formation similar to that observed in PDMS compounds can be found in the corona-treated fibers. This technique has the advantage that the beam can be focused onto the surface of the individual fibers. The Si–O peak at 550–450 cm^{-1} and the symmetric CH_3 stretching peak at 2960 cm^{-1} were used to determine the ratio of Si–O to C–CH_3 of the virgin electrospun materials and of the electrospun surface after 30 min of corona treatment. Figure 10 shows the ratio of these peaks for the electrospun fibers of different PDMS content before and after 30-min corona treatment. In all cases, the samples show an increase in the Si–O/C–CH_3 ratio after corona exposure. This is consistent with the enrichment of oxygen on the surface and the formation of a brittle silica-like layer that is observed in the SEM images and is similar to the degradation layer that is formed in pure PDMS compounds after corona exposure.

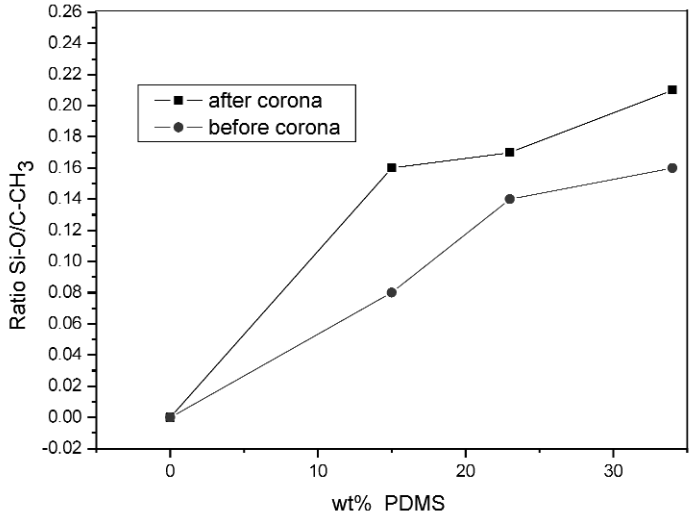

Fig. 10 Si–O/C–CH_3 ratio determined from Raman spectra for the Si–O 550–450 cm^{-1} to CH_3 2960 cm^{-1} peak heights for the fiber surfaces before and after 30-min corona treatment.

CONCLUSIONS

It has been shown that it is possible to produce polymer fibers of organic–inorganic polymers based on PMMA and PDMS using the electrospinning process. A series of PMMA-*g*-PDMS copolymers were synthesized with various PDMS content. The electrospinning conditions have a dramatic effect on the fiber diameters and morphology. In addition, the PDMS wt % also has a dramatic effect on the fiber morphology. The electrospun copolymer surfaces show considerably higher SCA values relative to the copolymer films. These surfaces produce superhydrophobic surfaces. The superhydrophobicity is not only a result of the increased surface roughness but also of the increased surface areas where the nanofiber series shows a greater dependence on the PDMS content than the corresponding polymer films. There is also a greater dependence of the SCA value of the electrospun surfaces with the PDMS content than on the average fiber diameter, suggesting that in this series the surface energy of the fibers dominates in determining the SCA over the basic fiber morphology (fiber diameter). In fact, the series shows a progressively more hydrophobic surface with an increase in the PDMS contents despite the increasing fiber diameter (and, therefore, less rough surface).

Exposure of the superhydrophobic fiber surfaces to corona discharges results in a complete loss of the superhydrophobicity where a water drop is completely absorbed into the fiber surface immediately after corona treatment. This loss of hydrophobicity is a result of the dramatic change in the fiber surface energy as a result of the chemical modification. SEM and confocal Raman spectroscopy confirm the surface modification due to the corona exposure. The loss of hydrophobicity is observed despite the fact that much of the surface roughness is preserved after the corona exposure. Samples treated for times less than 30 min show the phenomena of hydrophobicity recovery. The rate of recovery depends on the treatment time and the PDMS content of the fibers. Despite the recovery observed in these cases, none of the samples returned to their superhydrophobic state after corona treatment but instead recover to SCA of about 120° after 24 h. Evidence for a brittle "silica-like" degradation layer, similar to that observed in pure PDMS compounds, is found on the surface of the fibers after corona treatment.

ACKNOWLEDGMENTS

The authors would like to thank Prof. Mikael Hedenqvist of the Swedish Royal Institute of Technology (KTH) for providing access to confocal Raman analysis. This research is supported by the South African National Research Foundation (NRF) under grant no. FA2004042000053.

REFERENCES

1. M. Callies, D. Quéré. *Soft Matter* **1**, 55 (2005).
2. Y. C. Jung, B. Bhushan. *Nanotechnology* **17**, 4970 (2006).
3. T. Onda, S. Shibuichi, N. Satoh, K. Tsujii. *Langmuir* **12**, 2125 (1996).
4. J. L. Zhang, J. A. Li, Y. C. Han. *Macromol. Rapid Commun.* **25**, 1105 (2004).
5. J. Y. Shiu, C. W. Kuo. In *Proceedings of SPIE - The International Society of Optical Engineering*, pp. 325–332 (2005).
6. M. H. Jin, X. J. Feng, J. M. Xi, J. Zhai, K. W. Cho. *Macromol. Rapid. Commun.* **26**, 1805 (2005).
7. K. Teshima, H. Sugimura, Y. Inoue, O. Takai, A. Takano. *Appl. Surf. Sci.* **244**, 619 (2005).
8. H. Yabu, M. Shimomura. *Chem. Mater.* **17**, 5231 (2005).
9. F. Shi, Z. Q. Wang, X. Zhang. *Adv. Mater.* **17**, 1005 (2005).
10. L. Xu, W. Chen, A. Mulchandani, Y. Yan. *Angew. Chem., Int. Ed.* **43**, 6009 (2005).
11. M. Ma, R. M. Hill, J. L. Lowery, S. V. Fridrikh, G. C. Rutledge. *Langmuir* **21**, 5549 (2005).
12. H. Yabu, M. Shimonura. *Chem. Mater.* **17**, 5231 (2005).
13. M. T. Khorasani, H. Mirzadeh, Z. Kermani. *Appl. Surf. Sci.* **242**, 339 (2005).
14. R. Blossey. *Nat. Mater.* **2**, 301 (2003).
15. M. Minglin, M. H. Randal. *Curr. Opin. Colloid Interface Sci.* 193 (2006).
16. J. M. Deitzel, J. Kleinmeyer, D. Harris. *Polymer* **42**, 261 (2001).
17. J. M. Deitzel, J. D. Kleinmeyer, J. K. Hirvonen. *Polymer* **42**, 8163 (2001).
18. J. M. Deitzel, W. Kosik, S. H. McKnight. *Polymer* **43**, 1025 (2002).
19. J. Doshi, D. H. Reneker. *J. Electrostat.* **35**, 151 (1995).
20. J. Lyons, C. Li, F. Ko. *Polymer* **45**, 7595 (2004).
21. L. Larrondo, R. S. Marley. *J. Polym. Sci., Part B: Polym. Phys*. **19**, 933 (1981).
22. L. Larrondo, R. S. Marley. *J. Polym. Sci., Part B: Polym. Phys*. **19**, 921 (1981).
23. L. Larrondo, R. S. Marley. *J. Polym. Sci., Part B: Polym. Phys*. **19**, 909 (1981).
24. T. Kawai, M. Akashima, S. Teramachi. *Polymer* **36**, 2851 (1995).
25. Y. Lee, I. Akiba, S. Akiyama. *J. Appl. Polym. Sci*. **87**, 375 (2003).
26. M. Wang, A. J. Hsieh, G. C. Rutledge. *Polymer* **46**, 3404 (2005).
27. A. Frenot, I. S. Chronakis. *Curr. Opin. Colloid Interface Sci.* **8**, 64 (2003).
28. A. Kiesow, J. Meinhardt, A. Heilmann. *Coating* **37**, 36 (2004).
29. S. M. Kassiriha, S. Tarbiat, M. A. Fard. "Effect of surface treatment methods on the surface tension of plastics", in *Advances in Plastics Technology*, 5th International Conference, Katowice, Poland (2003).
30. S. Suzer, A. Argun, O. Vatansever, O. Aral. *J. App. Polym. Sci.* **74**, 1846 (1999).
31. M. J. Owen, M. Gentle, T. Orbeck, D. E. Williams. *Polymer Surface Dynamics*, J. D. Andrade (Ed.), Plenum Press, New York (1988).
32. P. Smith, M. J. Owen. *J. Conf. Electr. Insul. Diel. Phen.* 829 (1992).
33. H. Hillborg, U. M. Gedde. *Polymer* **39**, 1991 (1997).
34. A. Toth, I. Bertoti, M. Blazso, G. Banhegyi, A. Bognar, X. Szaplonczay. *J. Appl. Polym. Sci.* **52**, 1293 (1994).
35. M. Morra, E. Occhiello, R. Marola, F. Garbassi, P. Humphrey, D. Johnson. *J. Colloid Interface Sci.* **11**, 137 (1990).
36. J. R. Hollahan. *J. Appl. Polym. Sci.* **14**, 2499 (1970).

37. R. Scott, S. R. Gaboury, M. W. Urban. *Structure Property Relations in Polymers*, American Chemical Society Symposium Series No. 236, M. W Urban, C. D. Craver (Eds.), American Chemical Society, Washington, DC (1993).
38. P. E. Mallon, C. J. Greyling, W. Vosloo, Y. C. Jean. *Radiat. Phys. Chem.* **68**, 453 (2003).
39. M. Meincken, T. A. Berhane, P. E. Mallon. *Polymer* **46**, 203 (2005).
40. C. J. Buchko, Y. Shen, D. C. Martin, L. C. Chen. *Polymer* **40**, 7397 (1999).
41. H. Fong, I. Chun, D. H. Reneker. *Polymer* **40**, 4585 (1999).
42. S. J. Hinder, C. Lowe, J. T. Maxted, J. F. Watts. *Prog. Org. Coat.* **54**, 104 (2005).
43. C. S. Ha, J. A. Gardella. *J. Macromol. Sci*. **45**, 1 (2005).
44. X. Chen, J. A. Gardella. *Macromolecules* **26**, 3778 (1993).